Abstracta

Ano XXV - N. 05

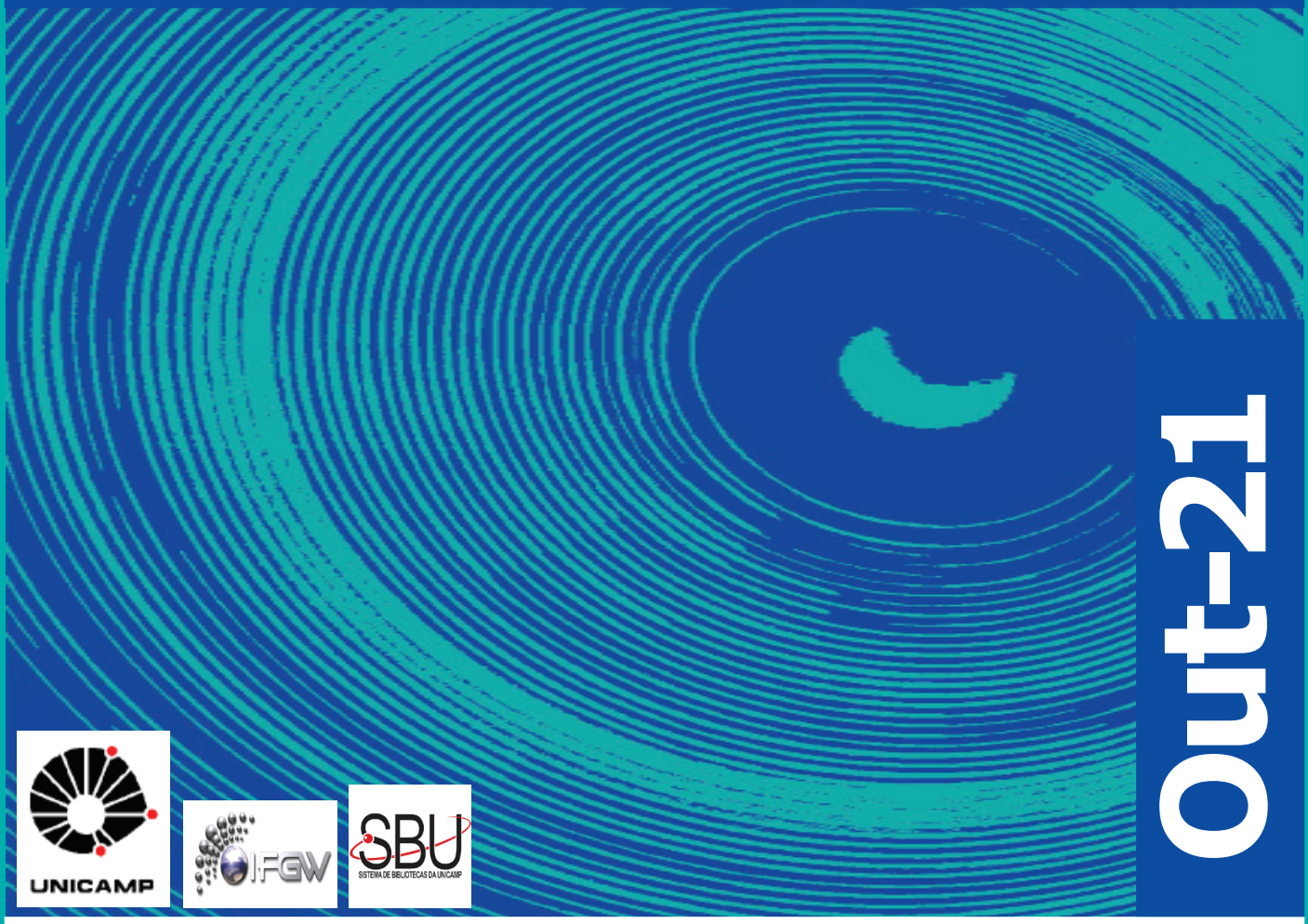

Out-21

UNICAMP

IFGW

SBU
SISTEMA DE BIBLIOTECAS DA UNICAMP

Artigos publicados
P200-2021 à P256-2021

Meeting Abstract
Me001-2021

Correções
Co007-2021 à Co008-2021

Defesas de Dissertações do IFGW
D016-2021 à D019-2021

Defesas de Teses do IFGW
T012-2021 à T013-2021

Artigos publicados

[P200-2021] "Anomalous Hall effect in bismuth"

Camargo, B. C.; Gierlowski, P.; **Alaferdov, A.*;** Demchenko, I. N.; Sawicki, M.; Gas, K.; **Kopelevich, Y.***

We report the occurrence of ferromagnetic-like anomalous Hall effect (AHE) below 30 mT in bismuth crystals. The signatures of ferromagnetism in transport are not corroborated in magnetization measurements, thus suggesting the induction of non-intrinsic magnetism at surfaces and grain boundaries in bismuth. The suppression of the AHE with the increase of magnetic field and temperature coincides with previous reports of superconductivity in Bi, suggesting an interplay between the two phenomena.

JOURNAL OF MAGNETISM AND MAGNETIC MATERIALS 525, 167581, 2021. DOI 10.1016/j.jmmm.2020.167581

[P201-2021] "Apparent Ferromagnetism in Exfoliated Ultrathin Pyrite Sheets"

Puthirath, A. B.; Balan, A. P.; **Oliveira, E. F.*;** Sreepal, V.; Hernandez, F. C. R.; Gao, G. H.; Chakingal, N.; Sassi, L. M.; Thibeorchews, P.; Costin, G.; Vajtai, R.; **Galvao, D. S.*;** Nair, R. R.; Ajayan, P. M.

There has been no experimental evidence for ferromagnetic ordering in isotropic atomically thin two-dimensional crystals, until a bilayer Cr2Ge2Te6 and a three-atom thick monolayer CrI3 is shown to retain ferromagnetic ordering at finite temperatures. Here, we demonstrate successful isolation of a nonvan der Waals-type ultrathin nanosheet of FeS2 derived from naturally occurring pyrite mineral (FeS2) by means of liquid-phase exfoliation. Structural characterizations imply that (111)-oriented sheets are predominant and are supported theoretically by means of density functional theory surface energy calculations. Spin-polarized density theory calculations further predicted that (111)-oriented three-atom thick pyrite sheets have a stable ferromagnetic ground state different from their diamagnetic bulk counterparts. This theoretical finding is evaluated by experimentally employing low-temperature superconducting quantum interference device measurements, and an anomalous ferromagnetic kind of behavior is observed.

JOURNAL OF PHYSICAL CHEMISTRY C 125[34], 18927-18935, 2021. DOI 10.1021/acs.jpcc.1c04977

[P202-2021] "Biocompatible Graphene Oxide Nanosheets Densely Functionalized with Biologically Active Molecules for Biosensing Applications"

Lehner, B. A. E.; Benz, D.; Moshkalev, S. A.; Meyer, A. S.; **Cotta, M. A.***; Janissen, R.

Graphene oxide (GO) has immense potential for widespread use in diverse in vitro and in vivo biomedical applications owing to its thermal and chemical resistance, excellent electrical properties and solubility, and high surface-to-volume ratio. However, development of GO-based biological nanocomposites and biosensors has been hampered by its poor intrinsic biocompatibility and difficult covalent biofunctionalization across its lattice. Many studies exploit the strategy of chemically modifying GO by noncovalent and reversible attachment of (bio)molecules or sole covalent biofunctionalization of residual moieties at the lattice edges, resulting in a low coating coverage and a largely bioincompatible composite. Here, we address these problems and present a facile yet powerful method for the covalent biofunctionalization of GO using colamine (CA) and the poly(ethylene glycol) cross-linker that results in a vast improvement in the biomolecular coating density and heterogeneity across the entire GO lattice. We further demonstrate that our biofunctionalized GO with CA as the cross-linker provides superior nonspecific biomolecule adhesion suppression with increased biomarker detection sensitivity in a DNA-biosensing assay compared to the (3-aminopropyl) triethoxysilane cross-linker. Our optimized biofunctionalization method will aid the development of GO-based in situ applications including biosensors, tissue nanocomposites, and drug carriers.

ACS APPLIED NANO MATERIALS 4[8], 8334-8342, 2021. DOI 10.1021/acsanm.1c01522

[P203-2021] "Coherent J/psi and psi ' photoproduction at midrapidity in ultra-peripheral Pb-Pb collisions at root s(NN)=5.02 TeV"

Acharya, S.; Adamova, D.; **Albuquerque, D. S. D.*; Chinellato, D. D.*; Takahashi, J.*;** et al. ALICE Collaboration

The coherent photoproduction of J/psi and psi' mesons was measured in ultra-peripheral Pb-Pb collisions at a center-of--mass energy root s(NN) = 5.02 TeV with the ALICE detector. Charmonia are detected in the central rapidity region for events where the hadronic interactions are strongly suppressed. The J/psi is reconstructed using the dilepton (l(+)l(-)) and proton-antiproton decay channels, while for the psi' the dilepton and the l(+)l(-) pi(+)pi(-) decay channels are studied. The analysis is based on an event sample corresponding to an integrated luminosity of about 233 mu b(-1). The results are compared with theoretical models for coherent J/psi and psi' photoproduction. The coherent cross section is found to be in a good agreement with models incorporating moderate nuclear gluon shadowing of about 0.64 at a Bjorken-x of around 6 x 10(-4), such as the EPS09 parametrization, however none of the models is able to fully describe the rapidity dependence of the coherent J/psi cross section including ALICE measurements at forward rapidity. The ratio of psi' to J/psi coherent photoproduction cross sections was also measured and found to be consistent with the one for photoproduction off protons.

EUROPEAN PHYSICAL JOURNAL C 81[8], 712, 2021. DOI 10.1140/epjc/s10052-021-09437-6

[P204-2021] "Compact dual-polarization silicon integrated couplers for multicore fibers"

Ruiz, J. L. P.*; Rocha, L. G.; Yang, J.; Kocabas, S. E.; Li, M. J.; Aldaya, I.; **Dainese, P.***; Gabrielli, L. H.

Compact fiber-to-chip couplers play an important role in optical interconnections, especially in data centers. However, the development of couplers has been mostly limited to standard single-mode fibers, with few devices compatible with multicore and multimode fibers. Through the use of state-of-the--art optimization algorithms, we designed a compact dual--polarization coupler to interface chips and dense multicore fibers, demonstrating, for the first time, coupling to both polarizations of all the cores, with measured coupling efficiency of -4.3 dB and with a 3 dB bandwidth of 48 nm. The dual--polarization coupler has a footprint of 200 mu m(2) per core, which makes it the smallest fiber-to-chip coupler experimentally demonstrated on a standard silicon-on-insulator platform.

OPTICS LETTERS 46[15], 3649-3652, 2021. DOI 10.1364/OL.425616

[P205-2021] "Constraints on the Initial State of Pb-Pb Collisions via Measurements of Z-Boson Yields and Azimuthal Anisotropy at root s(NN)=5.02 TeV"

Sirunyan, A. M; Tumasyan, A.; **Chinellato, J. A.*; Tonelli Manganote, E. J.***; et al. CMS Collaboration

The CMS experiment at the LHC has measured the differential cross sections of Z bosons decaying to pairs of leptons, as functions of transverse momentum and rapidity, in lead-lead collisions at a nucleon-nucleon center-of-mass energy of 5.02 TeV. The measured Z boson elliptic azimuthal anisotropy coefficient is compatible with zero, showing that Z bosons do not experience significant final-state interactions in the medium produced in the collision. Yields of Z bosons are compared to Glauber model predictions and are found to deviate from these expectations in peripheral collisions, indicating the presence of initial collision geometry and centrality selection effects. The precision of the measurement allows, for the first time, for a data-driven determination of the nucleon-nucleon integrated luminosity as a function of lead-lead centrality, thereby eliminating the need for its estimation based on a Glauber model.

PHYSICAL REVIEW LETTERS 127[10], 102002, 2021. DOI 10.1103/PhysRevLett.127.102002

[P206-2021] "Controlling the thermal switching in upconverting nanoparticles through surface chemistry"

Martinez, E. D.; **Garcia-Flores, A. F.***; Carneiro, A. N.; Brites, C. D. S.; Carlos, L. D.; **Urbano, R. R.*; Rettori, C.***

Photon upconversion taking place in small rare-earth-doped nanoparticles has been recently observed to be thermally modulated in an anomalous manner, showing thermal enhancement of the emission intensity. This effect was proved to be linked to the role of adsorbed water molecules as surface quenchers. The surface capping of the particles has a direct influence on the thermal dynamics of water adsorption and desorption, and therefore on the optical properties. Here, we show that the upconversion intensity of small-size (<25 nm) nanoparticles co-doped with Yb3+ and Er3+ ions, and functionalized with different capping molecules, presents clear irreversibility patterns upon thermal cycling that strongly depend on the chemical nature of the nanoparticle surface. By performing temperature-controlled luminescence measurements we observed the formation of a thermal hysteresis loop, resembling an optical switching phenomenon, whose shape and trajectory depend on the hydrophilicity of the surface. Additionally, an intensity overshoot takes place immediately after turning off the heating source, affecting each radiative transition differently. We performed numerical modelling to understand this effect considering non-radiative energy transfer from the surface defect states to the Er3+ ions. These findings are relevant for the comprehension of nanoparticle-based luminescence and the interplay between the surface and volume effects, and more generally, for applications involving UCNPs such as nanothermometry and bioimaging, and the development of optical encoding systems.

NANOSCALE, Acesso antecipado: AUG 2021. DOI 10.1039/d1nr03223b

[P207-2021] "Design and implementation of the AMIGA embedded system or data acquisition"

Aab, A.; Abreu, P.; **Chinellato, J. A.*; Franco D. de O.*; Dobrigkeit, C.*; Fauth, A. C.*; Payeras, A. M.*; Muller, M. A.***; et al. Pierre Auger Collaboration

The Auger Muon Infill Ground Array (AMIGA) is part of the AugerPrime upgrade of the Pierre Auger Observatory. It consists of particle counters buried 2.3 m underground next to the water-Cherenkov stations that form the 23.5 km(2) large infilled array. The reduced distance between detectors in this denser area allows the lowering of the energy threshold for primary cosmic ray reconstruction down to about 10(17) eV. At the depth of 2.3 m the electromagnetic component of cosmic ray showers is almost entirely absorbed so that the buried scintillators provide an independent and direct measurement of the air showers muon content.This work describes the design and implementation of the AMIGA embedded system, which provides centralized control, data acquisition and environment monitoring to its detectors. The presented system was firstly tested in the engineering array phase ended in 2017, and lately selected as the final design to be installed in all new detectors of the production phase. The system was proven to be robust and reliable and has worked in a stable manner since its first deployment.

JOURNAL OF INSTRUMENTATION 16[7], T07008, 2021. DOI 10.1088/1748-0221/16/07/T07008

[P208-2021] "Development and characterization of a water-based muon veto for the ν-Angra Experiment"

Souza, D. M.; Anjos, J. C.; Chimenti, P.; Costa, I. A.; Fernandes, A.; Guedes, G. P.; **Gonzalez, L. F. G.*; Kemp, E.***; Lima Jr, H. P.; Migliorini, M. L.; Nobrega, R. A.; Pepe, I. M.; Ribeiro, D. B. S.

The nu-Angra experiment has developed an antineutrino detector intended to operate at sea level, a few dozen meters from the core of a nuclear reactor. The operating principle of the detector is based on the water Cherenkov light detection to be in compliance with the safety rules of the power plant operator. The detector is exposed to a high rate of background events, mainly due to cosmic rays, making its veto system a key element for efficient background rejection. The nu-Angra Collaboration has designed a veto detector composed of three layers filled with water for both passive shielding and active detection of crossing particles. The veto surrounds a volume of 1.50 x 1.05 x 1.39 m(3), in which a target detector is placed, where the search for anti-neutrino events occurs. Any external particle hitting the detector must cross at least 25 cm of water before reaching this internal volume, which is protected by the veto structure, thus providing an important barrier against neutrons and low energy particles. In addition, the veto system has been instrumented with eight 8-inch photomultiplier tubes to detect external particles that may eventually reach the target detector. By making use of a trigger system based on scintillating paddles, energy distribution and detection efficiency of the veto system were assessed for different detector positions. This paper, therefore, presents the achieved results related to the characterization of such system concerning the detection of cosmic-ray muon particles passing through it.

NUCLEAR INSTRUMENTS & METHODS IN PHYSICS RESEARCH SECTION A-ACCELERATORS SPECTROMETERS DETECTORS AND ASSOCIATED EQUIPMENT 1004, 165378, 2021. DOI 10.1016/j.nima.2021.165378

[P209-2021] "Dynamical formation of graphene and graphane nanoscrolls"

Pereira Junior, M. L.; Ribeiro Junior, L. A.; **Galvao, D. S.***; Sousa, J. M. de

Carbon nanoscrolls (CNSs) are nanomaterials with geometry resembling graphene layers rolled up into a spiral (papyrus-like) form. Effects of hydrogenation and temperature on the self-scrolling process of two nanoribbons interacting with a carbon nanotube (CNT) have been studied by molecular dynamics simulations for three configurations: (1) graphene/graphene/CNT; (2) graphene/graphane/CNT, and (3) graphane/graphane/CNT. Graphane refers to a fully hydrogenated graphene nanoribbon. Nanoscroll formation is observed for configurations (1) and (2) for temperatures 300-1000 K, while nanoribbons wrap CNT without nanoscroll formation for configuration (3).

CHEMICAL PHYSICS LETTERS 780, 138919, 2021. DOI 10.1016/j.cplett.2021.138919

[P210-2021] "Effect of partial slip and radiation on liquid film fluid flow over an unsteady porous stretching sheet with viscous dissipation and heat source/sink"

Aslani, K. E.; Mahabaleshwar, U. S.; **Sakanaka, P. H.***; Sarris, I. E.

The effects of partial slip and heat transfer on an unsteady laminar boundary layer liquid film flow over a stretching surface with porous media subjected to radiation, viscous dissipation, and heat source/sink are reported. The time dependent laminar boundary layer equations are reduced to a nonlinear ordinary differential equation system with the use of similarity transformations. The flow and thermal fields are derived numerically using the efficient shooting method and plotted for various values of the relative dimensionless parameters, namely unsteadiness parameter S, the inverse Darcy number Da(-1), the slip parameter Gamma, the Prandtl number Pr, the heat source/sink parameter N-I, the thermal radiation parameter N-r and the Eckert number Ec. It was found that the temperature increases for increasing values of S, Da(-1), Gamma, N-r and heat source parameter (N-I > 0), whereas it decreases as Pr, Ec and heat sink parameter (N-I < 0) grow. Consequently, the velocity increases when S increases, while it is reduced as Da(-1) and Gamma grow.

JOURNAL OF POROUS MEDIA 24[11], 1-15, 045008.

[P211-2021] "Effect of Sodium Chloride on Internal Quasi--Liquid Layers in Ice I-h"

Ribeiro, I. D. A.*; Veiga, R. G. D.; **Koning, M. de***

We consider the effect of sodium chloride on the properties of internal interfaces in ice I-h. For this purpose, we employ molecular dynamics simulations to investigate the role of sodium and chloride ions in the properties of grain boundaries (GB), which are the interfacial regions separating adjacent crystal grains with different orientations. The results show that the presence of the ions significantly affects both the structural and dynamical characteristics of the disordered layers at the GB regions. Compared to pristine ice samples, in addition to reducing the degree of water structure, the ions enhance the mobility of the water molecules in the GB region. Even so, the briny GB regions display quasi-liquid behavior in that both the molecular and the ionic diffusivities are substantially lower than in the corresponding bulk liquid solutions at the same conditions of temperature, pressure, and salinity. Finally, the presence of sodium chloride in the GB regions is found to facilitate the GB sliding process, which is consistent with experimental insight.

JOURNAL OF PHYSICAL CHEMISTRY C 125[33], 18526-18535, 2021. DOI 10.1021/acs.jpcc.1c05461

[P212-2021] "Effects of the lower energy and pulse stacking in carbon dioxide laser skin treatment: an objective analysis using second harmonic generation"

Motta, M. M.; Stelini, R. F.; Calderoni, D. R.; Gilioli, R.; Damiani, G. V.; **Cesar, C. L.***; Kharmandayan, P.

Purpose: To evaluate the effect of fractional carbon dioxide (CO 2) laser treatment using lower power associated with pulse stacking within collagen fibers, using second harmonic generation microscopy and computerized image analysis. Methods: Twenty male Wistar rats aging eight weeks were used. Each treatment area received a single-pass CO2 fractional laser with different parameters. The 20 animals were divided into two groups and euthanized after 30 and 60 days. Second harmonic generation images were obtained and program ImageJ was utilized to evaluate the collagen organization within all areas. Collagen anisotropy, entropy and optical density were quantified. Results: Increased anisotropy over time was observed in all four areas, but only reached statistical significance (p = 0.0305) when the mildest parameters were used (area four). Entropy decreased over time in all areas, but without significance (p = 0.1779) in area four. Density showed an overtime increase only in area four, but no statistical significance was reached (p = 0.6534). Conclusion: When combined, the results obtained in this study regarding anisotropy, entropy and density tend to demonstrate that it is possible to achieve collagen remodeling with the use of lower power levels associated with stacked pulses.

ACTA CIRURGICA BRASILEIRA 36[3], e360304, 2021. DOI 10.1590/ACB360304

[P213-2021] "Emergence of fractional quantum mechanics in condensed matter physics"

Dartora, C. A.; Zanella, F.; **Cabrera, G. G.***

Condensed matter provides a fertile ground for the emergence of exotic phenomena. For instance, polymers typically lack long range order and crystalline symmetry, leading to difficulties in establishing a general theory to describe the properties of these materials. They exhibit memory, some extent of self--similarity and non-locality effects, which are better described by fractional calculus. In this letter we demonstrate the emergence of an effective Hamiltonian possessing fractional dispersion taking as the starting point a tight-binding model in which the hopping parameters from next-nearest neighbours cannot be neglected. Our model was applied to describe the Pauli paramagnetism in a system with fractional dispersion, the magnetic susceptibility of vanadyl acetate and the electronic transport as a function of temperature in conductive polymers, displaying good agreement between theory and experimental data.

PHYSICS LETTERS A 415, 127643, 2021. DOI 10.1016/j.physleta.2021.127643

[P214-2021] "Energy dependence of phi meson production at forward rapidity in pp collisions at the LHC"

Acharya, S.; Adamova, D.; **Albuquerque, D. S. D.*; Chinellato, D. D.*; Takahashi, J.***; et al. ALICE Collaboration

The production of phi mesons has been studied in pp collisions at LHC energies with the ALICE detector via the dimuon decay channel in the rapidity region 2.5 < y < 4. Measurements of the differential cross section d(2)sigma/dyd p(T) are presented as a function of the transverse momentum (p(T)) at the center-of--mass energies root s = 5.02, 8 and 13 TeV and compared with the ALICE results at midrapidity. The differential cross sections at root s = 5.02 and 13 TeV are also studied in several rapidity intervals as a function of p(T), and as a function of rapidity in three pT intervals. A hardening of the p(T)-differential cross section with the collision energy is observed, while, for a given energy, p(T) spectra soften with increasing rapidity and, conversely, rapidity distributions get slightly narrower at increasing p(T). The new results, complementing the published measurements at root s = 2.76 and 7 TeV, allow one to establish the energy dependence of phi meson production and to compare the measured cross sections with phenomenological models. None of the considered models manages to describe the evolution of the cross section with p(T) and rapidity at all the energies.

EUROPEAN PHYSICAL JOURNAL C 81[8], 772, 2021. DOI 10.1140/epjc/s10052-021-09545-3

[P215-2021] "Energy Evolution, Stabilization, and Mechanotransducer Properties of Fe3O4 Vortex Nanorings and Nanodisks"

Niraula, G.; Toneto, D.; Joshy, E.; Coaquira, J. A. H.; Ayesh, A. I.; Garcia, F.; **Muraca, D.*;** Denardin, J. C.; Goya, G. F.; Sharma, S. K.

Recent reports on spin structures produced in nanomaterials due to confinement of spins imposed by geometrical restrictions are at the center of rising scientific interest. Topological curling magnetic structures (vortices) exhibit unique properties, regarding the energy profile, good colloidal stability in suspensions, manipulation under a low-frequency magnetic field, and torque exertion. The last prop-erty provides the potential to mechanically eradicate cancer cells via magneto-mechanical actuation using remote ac magnetic fields. Here, we study, theoretically and by micromagnetic simulations, the mag-netic energy evolutions for vortex nanosystems, i.e., Fe3O4 nanodisks (NDs) and nanorings (NRs). The obtained results for magnetic energy, magnetic susceptibility, and magnetization reversal confirm that the vortex-domain structure in NRs exhibits better stability and avoids agglomeration in solution, owing to the presence of a central hole, whereas the presence of a vortex core in NDs induces magnetic remanence. Although NDs are found to exert slightly higher torques than NRs, this weakness can be compensated for by a small increase (i.e., approximately equals 20%) in the amplitude of the applied field. Our results provide evidence of the magnetic stability of the curling ground states in NRs and open the possibility of applying these systems to magnetomechanical actuation on single cells for therapeutics in biomedicine, such as cancer-cell destruction by low-frequency torque transduction.

PHYSICAL REVIEW APPLIED 16[2], 024002, 2021. DOI 10.1103/PhysRevApplied.16.024002

[P216-2021] "First-principles study of solid-state properties of adrenergic neurotransmitters, orthorhombic noradrenaline, and monoclinic adrenaline"

Araujo, R. L.; Lima Neto, J. X.; Barboza, C. A.; Oliveira, J. I. N.; **Tromer, R. M.*;** Henriques, J. M.; Fulco, U. L.

Using the density functional theory with the approximation of the generalized gradient approximation, we carried out a theoretical investigation of the structural, optoelectronic, vibrational (IR and Raman), and thermodynamic properties of the noradrenaline (NA) and adrenaline (AD) crystals. The lattice parameters showed good agreement with the experimental data, and an indirect bandgap was obtained for both structures. The calculated optical properties showed that the crystal of noradrenaline has a slightly higher sensitivity than adrenaline, and the absorption of both crystalline structures occurs in the UV region, showing greater sensitivity to electromagnetic radiation with an energy of approximately 5 eV and a dielectric constant of approximately 2.50 for NA and AD. Finally, IR and Raman spectra were presented, and a thermodynamic analysis showed that the adrenaline crystal is more stable than the noradrenaline crystal as the temperature increases.

JOURNAL OF APPLIED PHYSICS 129[23], 234702, 2021. DOI 10.1063/5.0054383

[P217-2021] "General approach for anisotropic magnetoresistance calculations used for revealing the role of cobalt nanowire?s geometrical details"

Velo, M. F.*; Santos, M. V. P. dos*; Cecchi, B. M.*; Pirota, K. R.*

The electrical resistivity modulation by the application of external magnetic fields, known as magnetoresistance effect (MR), is a widely studied subject driven by both technological applications and fundamental challenges, although being difficult to make numerical predictions from first analytical principles. In this work, we present a MR simulator protocol that combines micromagnetics with classical electrodynamics and works well for room temperature anisotropic magnetoresistance (AMR) for a large magnetic field variation range. As a proof of concept, we applied it to simulate the AMR of a previously reported Co-C composite nanostructure defined by a central nanostripe as the current line with transversal voltage contacts. In addition to the macroscopic measurable quantities like average magnetization and MR signal, the method returns the microscopic spatial magnetization distribution and gives insights about the magnetization reversal mechanism. For example, for this particular case, the magnetic domain walls are predominantly nucleated near the magnetic voltage terminals and their propagation features are the main responsible for the MR observed behavior. Other elements can be easily incorporated to the protocol in order to simulate materials with additional complexities such as crystalline grains or magnetocrystalline anisotropy.

JOURNAL OF MAGNETISM AND MAGNETIC MATERIALS 532, 167945, 2021. DOI 10.1016/j.jmmm.2021.167945

[P218-2021] "Hard color-singlet exchange in dijet events in proton-proton collisions at root s=13 TeV"

Sirunyan, A. M; Tumasyan, A.; **Chinellato, J. A.*; Tonelli Manganote, E. J.***; et al. CMS Collaboration

Events where the two leading jets are separated by a pseudorapidity interval devoid of particle activity, known as jet-gap-jet events, are studied in proton-proton collisions at root s = 13 TeV. The signature is expected from hard color-singlet exchange. Each of the highest transverse momentum (p(T)) jets must have p(T)(jet) > 40 GeV and pseudorapidity 1.4 < vertical bar eta(jet)vertical bar < 4.7, with eta(jet1)eta(jet2) < 0, where jet1 and jet2 are the leading and subleading jets in p(T), respectively. The analysis is based on data collected by the CMS and TOTEM experiments during a low luminosity, high-beta* run at the CERN LHC in 2015, with an integrated luminosity of 0.66 pb(-1). Events with a low number of charged particles with p(T) > 0.2 GeV in the interval vertical bar eta vertical bar < 1 between the jets are observed in excess of calculations that assume only color-exchange. The fraction of events produced via color-singlet exchange, f(CSE), is measured as a function of p(T)(jet2), the pseudorapidity difference between the two leading jets, and the azimuthal angular separation between the two leading jets. The fraction f(CSE) has values of 0.4-1.0%. The results are compared with previous measurements and with predictions from perturbative quantum chromodynamics. In addition, the first study of jet-gap-jet events detected in association with an intact proton using a subsample of events with an integrated luminosity of 0.40 pb(-1) is presented. The intact protons are detected with the Roman pot detectors of the TOTEM experiment. The f(CSE) in this sample is 2.91 +/- 0.70(stat)(-1.01)(+1.08)(syst) times larger than that for inclusive dijet production in dijets with similar kinematics.

PHYSICAL REVIEW D 104[3], 032009, 2021. DOI 10.1103/PhysRevD.104.032009

[P219-2021] "Improving the Room-Temperature Ferromagnetism in ZnO and Low-Doped ZnO:Ag Films Using GLAD Sputtering"

Correa, M. A.; Ferreira, A.; **Tromer, R. M.***; Machado, L. D.; Gamino, M.; Franca Junior, S. A. N.; Bohn, F.; Vaz, F.

ZnO and doped ZnO films with non-ferromagnetic metal have been widely used as biosensor elements. In these studies, the electrochemical measurements are explored, though the electrical impedance of the system. In this sense, the ferromagnetic properties of the material can be used for multifunctionalization of the sensor element using external magnetic fields during the measurements. Within this context, we investigate the room-temperature ferromagnetism in pure ZnO and Ag--doped ZnO films presenting zigzag-like columnar geometry. Specifically, we focus on the films' structural and quasi-static magnetic properties and disclose that they evolve with the doping of low-Ag concentrations and the columnar geometry employed during the deposition. The magnetic characterization reveals ferromagnetic behavior at room temperature for all studied samples, including the pure ZnO one. By considering computational simulations, we address the origin of ferromagnetism in ZnO and Ag-doped ZnO and interpret our results in terms of the Zn vacancy dynamics, its substitution by an Ag atom in the site, and the influence of the columnar geometry on the magnetic properties of the films. Our findings bring to light an exciting way to induce/explore the room-temperature ferromagnetism of a non-ferromagnetic metal-doped semiconductor as a promising candidate for biosensor applications.

MATERIALS 14[18], 5337, 2021. DOI: 10.3390/ma14185337

[P220-2021] "Influence of substrate bias and temperature on the crystallization of metallic NbTaTiVZr high-entropy alloy thin films"

Cemin, F.*; Mello, S. R. S. de*; Figueroa, C. A.; **Alvarez, F.***

Metallic sputtered high-entropy alloy (HEA) thin films often result in amorphous structures, due to the film growth kinetics and the large atomic size mismatch of the constituent elements. In this paper, single-phase crystalline NbTaTiVZr HEA thin films were achieved by the appropriate choice of both the alloying elements and the synthesis conditions. Regarding the latter, substrate biasing prompts Ar+ ion irradiation during film growth, whereas substrate heating increases the adatom mobility, inducing specific structural modifications. The control of both variables eliminates traditional crystallization strategies, such as adding nitrogen to the gas mixture during film growth or post-thermal annealing of the as-deposited films. Therefore, we have investigated the relationship between the synthesis conditions, the structure, and the mechanical properties of a Nb20Ta26-Ti22V16Zr16 HEA thin film, due to its potential application in the field of refractory coating materials. The asdeposited films prepared at 400 degrees C possessed a body-centered cubic (bcc) phase, and their preferential orientation changed according to the bias voltage value (V-b) chosen. Low energy ion irradiation (V-b approximate to -25 V) resulted in crystallite coarsening and surface roughening. On the other hand, higher negative bias voltages (V-b approximate to -75 V) led to lower growth rates, grain refining, and improved mechanical properties. In addition, the chemical states and composition were determined by X-ray photoelectron spectroscopy (XPS) and the HEA phase formation was predicted using empirical parameters and compared to the results obtained by the Calculation of Phase Diagrams (CALPHAD) approach.

SURFACE & COATINGS TECHNOLOGY 421, 127357, 2021. DOI: 10.1016/j.surfcoat.2021.127357

[P221-2021] "Information Scrambling versus Decoherence--Two Competing Sinks for Entropy"

Touil, A.; **Deffner, S.***

A possible solution of the information paradox can be sought in quantum information scrambling. In this paradigm, it is postulated that all information entering a black hole is rapidly and chaotically distributed across the event horizon, making it impossible to reconstruct the information by means of any local measurement. However, in this scenario, the effects of decoherence are typically ignored, which may render information scrambling moot in cosmological settings. In this work, we develop key steps toward a thermodynamic description of information scrambling in open quantum systems. In particular, we separate the entropy change into contributions arising from scrambling and decoherence, for which we derive statements of the second law. This is complemented with a numerical study of the SachdevYe-Kitaev, Maldacena-Qi, XXX, mixed-field Ising, and Lipkin-Meshkov-Glick models in the presence of decoherence in the energy or in the computational basis.

PRX QUANTUM 2[1], 010306, 2021. DOI 10.1103/PRXQuantum.2.010306

[P222-2021] "Low energy alpha particle tracks in CR-39 nuclear track detectors: Chemical etching studies"

Oliveira, C. S.; Malheiros, B.; Pires, K. C. C.; Assuncao, M.; **Guedes, S.***; Correa, J. N.; Paschuk, S. A.

The widely known CR-39 nuclear track detectors (NTDs) have been used to investigate the etch pits formed by alpha particles from a Am-241 source moderated to 1-2 MeV. The efficiencies of two available CR-39 plastic detectors, Lantrak and Baryotrak, have been studied as a function of the chemical etching time. The chemical etching solutions of the NaOH, KOH and NaOH+ethyl alcohol at 70 and 80 degrees C have been applied to build etch pit diameter growths as well as density curves. The obtained growth curves of etch pit diameters have been compared under these different etching conditions, showing similar general trends for Baryotrak and Lantrak detectors for etching at 70 degrees C. A slight divergence of the curves have been observed at 80 degrees C for etching times above 400 min, revealing a small variation in the bulk etch rates between the two detector types. The etch pit density curves for both detectors have also been studied, showing a plateau for all etching conditions except for NaOH+ethyl alcohol at 80 degrees C, in which there is a significant decrease in density after approximate to 600 min of etching. The results obtained with the protocols described in detail in this work show the pertinent precautions to be adopted in the chemical treatment of NTDs for the detection of alpha particle at low energies. In particular, the quantitative results highlight the limits of linear growth of pits and induction etching time for etch pits with diameters D=0 mu m (EIT0) and D=1 mu m (EIT1).

NUCLEAR INSTRUMENTS & METHODS IN PHYSICS RESEARCH SECTION A-ACCELERATORS SPECTROMETERS DETECTORS AND ASSOCIATED EQUIPMENT 995, 165130, 2021. DOI 10.1016/j.nima.2021.165130

[P223-2021] "Macroscopic-ranged proximity effect in graphite"

Camargo, B. C.; Gierlowski, P.; Kuzmiak, M.; Jesus, R. F. de; Onufriienko, O.; Szabo, P.; **Kopelevich, Y.***

We report proximity-induced superconducting features over macroscopic lengths in highly oriented pyrolytic graphite. The phenomenon is triggered when electrical currents are injected in the material through superconducting electrodes, few millimeters apart from each other. Such a large range is anomalous, as proximity-induced features in normal conductors hardly surpass few micrometers. The results can be explained as due to the presence of pre-existing superconductivity in graphite on small, localized regions.

JOURNAL OF PHYSICS-CONDENSED MATTER 33[49], 495602, 2021. DOI: 10.1088/1361-648X/ac24c5

[P224-2021] "Measurements of angular distance and momentum ratio distributions in three-jet and Z plus two-jet final states in pp collisions"

Sirunyan, A. M; Tumasyan, A.; **Chinellato, J. A.*; Tonelli Manganote, E. J.***; et al. CMS Collaboration

Collinear (small-angle) and large-angle, as well as soft and hard radiations are investigated in three-jet and Z + two--jet events collected in proton-proton collisions at the LHC. The normalized production cross sections are measured as a function of the ratio of transverse momenta of two jets and their angular separation. The measurements in the three--jet and Z + two-jet events are based on data collected at a center-of-mass energy of 8 TeV, corresponding to an integrated luminosity of 19.8 fb(-1). The Z + two-jet events are reconstructed in the dimuon decay channel of the Z boson. The three-jet measurement is extended to include root s = 13 TeV data corresponding to an integrated luminosity of 2.3 fb(-1). The results are compared to predictions from event generators that include parton showers, multiple parton interactions, and hadronization. The collinear and soft regions are in general well described by parton showers, whereas the regions of large angular separation are often best described by calculations using higher-order matrix elements.

EUROPEAN PHYSICAL JOURNAL C 81[9], 852, 2021. DOI: 10.1140/epjc/s10052-021-09570-2

[P225-2021] "Modeling neutral viral mutations in the spread of SARS-CoV-2 epidemics"

Marquioni, V. M.*; Aguiar, M. A. M.*

Although traditional models of epidemic spreading focus on the number of infected, susceptible and recovered individuals, a lot of attention has been devoted to integrate epidemic models with population genetics. Here we develop an individual--based model for epidemic spreading on networks in which viruses are explicitly represented by finite chains of nucleotides that can mutate inside the host. Under the hypothesis of neutral evolution we compute analytically the average pairwise genetic distance between all infecting viruses over time. We also derive a mean-field version of this equation that can be added directly to compartmental models such as SIR or SEIR to estimate the genetic evolution. We compare our results with the inferred genetic evolution of SARS-CoV-2 at the beginning of the epidemic in China and found good agreement with the analytical solution of our model. Finally, using genetic distance as a proxy for different strains, we use numerical simulations to show that the lower the connectivity between communities, e.g., cities, the higher the probability of reinfection.

PLOS ONE 16[7], e0255438, 2021. DOI 10.1371/journal.pone.0255438

[P226-2021] "Multiharmonic Correlations of Different Flow Amplitudes in Pb-Pb Collisions at root s(NN)=2.76 TeV"

Acharya, S.; Adamova, D.; **Albuquerque, D. S. D.*; Chinellato, D. D.*; Takahashi, J.***; et al. ALICE Collaboration

The event-by-event correlations between three flow amplitudes are measured for the first time in Pb-Pb collisions, using higher-order symmetric cumulants. We find that different three-harmonic correlations develop during the collective evolution of the medium when compared to correlations that exist in the initial state. These new results cannot be interpreted in terms of previous lower-order flow measurements since contributions from two-harmonic correlations are explicitly removed in the new observables. A comparison to Monte Carlo simulations provides new and independent constraints for the initial conditions and system properties of nuclear matter created in heavy-ion collisions.

PHYSICAL REVIEW LETTERS 127, 092302, 2021. DOI 10.1103/PhysRevLett.127.092302

[P227-2021] "MUSiC: a model-unspecific search for new physics in proton-proton collisions at root s=13TeV"

Sirunyan, A. M; Tumasyan, A.; **Chinellato, J. A.*; Tonelli Manganote, E. J.***; et al. CMS Collaboration

Results of the Model Unspecific Search in CMS (MUSiC), using proton-proton collision data recorded at the LHC at a centre--of-mass energy of 13 TeV, corresponding to an integrated luminosity of 35.9 fb(-1), are presented. The MUSiC analysis searches for anomalies that could be signatures of physics beyond the standard model. The analysis is based on the comparison of observed data with the standard model prediction, as determined from simulation, in several hundred final states and multiple kinematic distributions. Events containing at least one electron or muon are classified based on their final state topology, and an automated search algorithm surveys the observed data for deviations from the prediction. The sensitivity of the search is validated using multiple methods. No significant deviations from the predictions have been observed. For a wide range of final state topologies, agreement is found between the data and the standard model simulation. This analysis complements dedicated search analyses by significantly expanding the range of final states covered using a model independent approach with the largest data set to date to probe phase space regions beyond the reach of previous general searches.

EUROPEAN PHYSICAL JOURNAL C 81[7], 629, 2021. DOI 10.1140/epjc/s10052-021-09236-z

[P228-2021] "New Transition and Energy Levels of Three--Times Ionized Krypton (Kr IV)"

Raineri, M.; Gallardo, M.; Almandos, J. R.; **Trigueiros, A. G.***; Pagan, C. J. B.

A capillary pulsed-discharge and a theta-pinch were used to record Kr spectra in the region of 330-4800 angstrom. A set of 168 transitions of these spectra were classified for the first time. We extended the analysis to twenty-five new energy levels belonging to 3s(2)3p(2)4d, 3s(2)3p(2)5d even configurations. We calculated weighted transition probabilities (gA) for all of the experimentally observed lines and lifetimes for new energy levels using a relativistic Hartree-Fock method, including core-polarization effects.

ATOMS 9[3], 48, 2021. DOI: 10.3390/atoms9030048

[P229-2021] "On the physical and electrochemical properties of MLG-based electrode surfaces modified by microwave-assisted reactive plasma"

Moura, G. D. de; Silva, C. C. da; Naves, E. A. A.; Moreto, J. A.; Ferreira, D. C.; Oliveira, P. R. de; Kalinke, C.; Scarminio, J.; **Siervo, A. de***; Cunha, T. H. R. da; Gelamo, R. V.

The reactive plasma technique is often employed to activate the surface of materials both chemically and physically. Considering that several parameters should be handled in a plasma treatment process, a multivariate experimental design of three factors in two levels was employed to define the plasma treatment configurations under which the MLG were submitted.

Plasma intensity, partial pressure of oxygen and reaction time were employed in the experimental planning. The surface morphology, the generation of C-C bond defects, surface chemical composition, interfacial free energy, and electrochemical properties were analyzed for the MLG electrodes as a function of the plasma treatment parameters. The treatments effectively promoted the MLG electrode's surface activation, considering the results obtained, which showed a dependence on those plasma treatment variables. The results suggested that plasma treatment variable adjustments can be used to modulate specific surface properties and with potential applicability in electrochemical sensors and supercapacitors.

MATERIALS SCIENCE AND ENGINEERING B-ADVANCED FUNCTIONAL SOLID-STATE MATERIALS 272, 115346, 2021. DOI: 10.1016/j.mseb.2021.115346

[P230-2021] "Phototribology: Control of Friction by Light"

Perotti, B. L.; Cammarata, A.; **Cemin, F.*; Mello, S. R. S. de***; Leidens, L. M.; **Echeverrigaray, F. G.***; Minea, T.; **Alvarez, F.***; Michels, A. F.; Polcar, T.; Figueroa, C. A.

In dry sliding, the coefficient of friction depends on the material pair and contact conditions. If the material and operating conditions remain unchanged, the coefficient of friction is constant. Obviously, we can tune friction by surface treatments, but it is a nonreversible process. Here, we report active control of friction forces on TiO2 thin films under UV light. It is reversible and stable and can be tuned/controlled with the light wavelength. The analysis of atomic force microscopy signals by wavelet spectrograms reveals different mechanisms acting in the darkness and under UV. Ab initio simulations on UV light-exposed TiO2 show a lower atomic orbital overlapping on the surface, which leads to a friction reduction of up to 60%. We suggest that photocontrol of friction is due to the modification of atomic orbital interactions from both surfaces at the sliding interface.

ACS APPLIED MATERIALS & INTERFACES 13[36], 43746-43754, 2021. DOI 10.1021/acsami.1c13054

[P231-2021] "Polyethyleneimine-Functionalized Carbon Nanotube/Graphene Oxide Composite: A Novel Sensing Platform for Pb(II) Acetate in Aqueous Solution"

Jimenez, M. J. M.*; Avila, A.; Barros, A. de; Lopez, E. O.; **Alvarez, F.*; Riul Jr., A.***; Perez-Taborda, J. A.

Heavy metal pollution is posing a severe health risk on living organisms. Therefore, significant research efforts are focused on their detection. Here, we developed a sensing platform sensor for the selective detection of lead(II) acetate. The sensor is based on self-assembled polyethyleneimine-functionalized carbon nanotubes (PEI-CNTs) and graphene oxide films deposited onto gold interdigitated electrodes. The graphene-based nanostructure showed a resistive behavior, and the fabricated layer-by-layer film was used to detect Pb(II) acetate in an aqueous solution by comparison of three electrochemical methods: impedance spectroscopy, amperometry, and potentiometry stripping analysis. The results obtained from different methods show that the detection limit was down to 36 pmol/L and the sensitivity up to 4.3 mu AL/mu mol, with excellent repeatability. The detection mechanism was associated with the high affinity of heavy metal ions with the functional groups present in the PEI-CNTs and GO, allowing high performance and sensitivity. The achieved results are important for the research toward integrated monitoring and sensing platforms for Pb(II) contamination in drinking water.

ACS OMEGA 6[28], 18190-18199, 723. 2021. DOI 10.1021/acsomega.1c02085

[P232-2021] "Precision luminosity measurement in proton--proton collisions at root S=13 TeV in 2015 and 2016 at CMS"

Sirunyan, A. M; Tumasyan, A.; **Chinellato, J. A.*; Tonelli Manganote, E. J.*** et al. CMS Collaboration

The measurement of the luminosity recorded by the CMS detector installed at LHC interaction point 5, using proton-proton collisions at root S = 13 TeV in 2015 and 2016, is reported. The absolute luminosity scale is measured for individual bunch crossings using beam-separation scans (the van der Meer method), with a relative precision of 1.3 and 1.0% in 2015 and 2016, respectively. The dominant sources of uncertainty are related to residual differences between the measured beam positions and the ones provided by the operational settings of the LHC magnets, the factorizability of the proton bunch spatial density functions in the coordinates transverse to the beam direction, and the modeling of the effect of electromagnetic interactions among protons in the colliding bunches. When applying the van der Meer calibration to the entire run periods, the integrated luminosities when CMS was fully operational are 2.27 and 36.3 fb(-1) in 2015 and 2016, with a relative precision of 1.6 and 1.2%, respectively. These are among the most precise luminosity measurements at bunched-beam hadron colliders.

EUROPEAN PHYSICAL JOURNAL C 81[9], 800, 2021. DOI 10.1140/epjc/s10052-021-09538-2

[P233-2021] "Production of pions, kaons, (anti-)protons and phi mesons in Xe-Xe collisions at sNN=5.44 TeV"

Acharya, S.; Adamova, D.; **Albuquerque, D. S. D.*; Chinellato, D. D.*; Takahashi, J.*;** et al. ALICE Collaboration

The first measurement of the production of pions, kaons, (anti-)protons and phi mesons at midrapidity in Xe-Xe collisions at root 5.44 TeV is presented. Transverse momentum (pT) spectra and pT-integrated yields are extracted in several centrality intervals bridging from p-Pb to mid-central Pb--Pb collisions in terms of final-state multiplicity. The study of Xe-Xe and Pb-Pb collisions allows systems at similar charged--particle multiplicities but with different initial geometrical eccentricities to be investigated. A detailed comparison of the spectral shapes in the two systems reveals an opposite behaviour for radial and elliptic flow. In particular, this study shows that the radial flow does not depend on the colliding system when compared at similar charged-particle multiplicity. In terms of hadron chemistry, the previously observed smooth evolution of particle ratios with multiplicity from small to large collision systems is also found to hold in Xe-Xe. In addition, our results confirm that two remarkable features of particle production at LHC energies are also valid in the collision of medium-sized nuclei: the lower proton-to-pion ratio with respect to the thermal model expectations and the increase of the phi-to-pion ratio with increasing final-state multiplicity.

EUROPEAN PHYSICAL JOURNAL C 81[7] 584, 2021. DOI 10.1140/epjc/s10052-021-09304-4

[P234-2021] "Pseudorapidity distributions of charged particles as a function of mvid- and forward rapidity multiplicities in pp collisions at root s=5.02, 7 and 13 TeV"

Acharya, S.; Adamova, D.; **Albuquerque, D. S. D.*; Chinellato, D. D.*; Takahashi, J.***; et al. ALICE Collaboration

Themultiplicity dependence of the pseudorapidity density of charged particles in proton-proton (pp) collisions at centre-of-mass energies root s = 5.02, 7 and 13 TeV measured by ALICE is reported. The analysis relies on track segments measured in the midrapidity range (|eta| < 1.5).

Results are presented for inelastic events having at least one charged particle produced in the pseudorapidity interval |eta| < 1. The multiplicity dependence of the pseudorapidity density of charged particles is measured with midand forward rapidity multiplicity estimators, the latter being less affected by autocorrelations. Adetailed comparison with predictions from the PYTHIA 8 and EPOS LHC event generators is also presented. The results can be used to constrain models for particle production as a function of multiplicity in pp collisions.

EUROPEAN PHYSICAL JOURNAL C 81[7], 630, 2021. DOI 10.1140/epjc/s10052-021-09349-5

[P235-2021] "Quantum and Classical Ergotropy from Relative Entropies"

Sone, A.; **Deffner, S.***

The quantum ergotropy quantifies the maximal amount of work that can be extracted from a quantum state without changing its entropy. Given that the ergotropy can be expressed as the difference of quantum and classical relative entropies of the quantum state with respect to the thermal state, we define the classical ergotropy, which quantifies how much work can be extracted from distributions that are inhomogeneous on the energy surfaces. A unified approach to treat both quantum as well as classical scenarios is provided by geometric quantum mechanics, for which we define the geometric relative entropy. The analysis is concluded with an application of the conceptual insight to conditional thermal states, and the correspondingly tightened maximum work theorem.

ENTROPY 23[9], 1107, 2021. DOI: 10.3390/e23091107

[P236-2021] "Quantum phase estimation with squeezed quasi-Bell states"

Souza, D. D. de*; Vidiella-Barranco, A.*

In this paper we present a study of the quantum phase estimation problem employing continuous-variable, entangled squeezed coherent (quasi-Bell) states as probe states. We show that their inherent squeezing and entanglement properties might bring advantages, increasing the precision of phase estimation compared to protocols which employ other continuous variable states e.g., two-mode, entangled coherent states or single-mode, squeezed states. We also analyze the phase estimation process considering: (i) a linear (unitary) perturbation, and (ii) dissipation, and conclude that the use of entangled squeezed coherent states as probe states may still be advantageous even under non-ideal conditions.

OPTIK 244, 167532, 2021. DOI 10.1016/j.ijleo.2021.167532

[P237-2021] "Reactive oxygen plasma treatment of 3D-printed carbon electrodes towards high-performance electrochemical sensors"

Pereira, J. F. S.; Rocha, R. G.; Castro, S. V. F.; Joao, A. F.; Borges, P. H. S.; Rocha, D. P.; **Siervo, A. de***; Richter, E. M.; Nossol, E.; Gelamo, R. V.; Munoz, R. A. A.

Conductive 3D-printed platforms have been recognized an emerging class of materials with great potential to electrochemistry. However, such 3D-printed electrodes require a surface treatment to remove excess of polymer that hinders the electron transfer. We report a fast (2-min) and chemical-free protocol for the surface treatment of 3D-printed conductive electrodes based on reactive cold oxygen plasma. A dramatic improvement of electrochemical activity of 3D-printed carbon black-polylactic acid (CB-PLA) electrodes was verified by the decrease in the peak-to-peak separation of the voltammetric response for the [Fe(CN)(6)](3-)/[Fe(CN)(6)](4-) couple and in the resistance of change transfer. The O-2 plasma treatment increased oxide groups and graphitic groups at the CB-PLA surface (verified by XPS) and provided higher rugosity (SEM images) thus higher exposure of conducting carbon sites and increased electroactive area in comparison with CO2-plasma, which explains the improved electrochemical performance using O-2-plasma treated electrodes. This protocol is faster and provided improved electrochemical activity compared with electrochemical, chemical, or biological treatments. As proofs-of concept, the benefits of surface plasma treatment of the 3D-printed electrodes were demonstrated towards the electrochemical sensing of dopamine and nitrite, molecules of biological interest, including the analysis of human saliva. Values of sensitivity and detection limit were greatly improved when using O-2 plasma treatment for both molecules (up to 100-fold increase in sensitivity for the voltammetric detection of dopamine), suggesting great promises for the development of highly-sensitive electrochemical sensors.

SENSORS AND ACTUATORS B-CHEMICAL 347, 130651, 2021. DOI 10.1016/j.snb.2021.130651

[P238-2021] "Reassessing the Adsorption Behavior and on-Surface Reactivity of a Brominated Porphyrin on Cu(111)"

Santos, A. C. dos*; Herrera-Reinoza, N.*; Paz, A. P.; Mowbray, D. J.; **Siervo, A. de***

On-surface coupling reactions and molecular conformation are essential processes for building tailored functional molecular nanostructures. Here, we study the thermal debromination and reactivity of free-base tetra(4-bromophenyl) porphyrin (H2T-BrPP) on Cu(111) as a function of the substrate temperature. It has been previously reported in the literature that C-Br bonds remain intact at room temperature (RT) and that the Br center dot center dot center dot Cu(111) interaction induces a drastic surface reconstruction around the molecule periphery and a distortion in the adsorbate itself. However, based on a combination of STM and XPS experiments, supported by density functional theory (DFT) calculations, we instead demonstrate that debromination readily occurs at RT, leading to a new interpretation of both the adsorption behavior and the molecular coupling of H2TBrPP on Cu(111). For the molecules deposited on the metallic substrate held above RT, our STM measurements show the growth of ordered 2D metal-organic frameworks (MOFs).

JOURNAL OF PHYSICAL CHEMISTRY C 125[31], 17164-17173, 2021. DOI 10.1021/acs.jpcc.1c03346

[P239-2021] "Search for a heavy vector resonance decaying to a Z boson and a Higgs boson in proton-proton collisions at s=13 Te"

Sirunyan, A. M; Tumasyan, A.; **Chinellato, J. A.*; Tonelli Manganote, E. J.***; et al. CMS Collaboration

A search is presented for a heavy vector resonance decaying into a Z boson and the standard model Higgs boson, where the Z boson is identified through its leptonic decays to electrons, muons, or neutrinos, and the Higgs boson is identified through its hadronic decays. The search is performed in a Lorentz-boosted regime and is based on data collected from 2016 to 2018 at the CERN LHC, corresponding to an integrated luminosity of 137 fb-1. Upper limits are derived on the production of a narrow heavy resonance Z ', and a mass below 3.5 and 3.7 Te is excluded at 95% confidence level in models where the heavy vector boson couples predominantly to fermions and to bosons, respectively.

These are the most stringent limits placed on the Heavy Vector Triplet Z ' model to date. If the heavy vector boson couples exclusively to standard model bosons, upper limits on the product of the cross section and branching fraction are set between 23 and 0.3 fb for a Z ' mass between 0.8 and 4.6 Te, respectively. This is the first limit set on a heavy vector boson coupling exclusively to standard model bosons in its production and decay.

EUROPEAN PHYSICAL JOURNAL C 81[8], 688, 2021. DOI 10.1140/epjc/s10052-021-09348-6

[P240-2021] "Search for charged Higgs bosons produced in vector boson fusion processes and decaying into vector boson pairs in proton-proton collisions at root s=13 TeV"

Sirunyan, A. M; Tumasyan, A.; **Chinellato, J. A.*; Tonelli Manganote, E. J.***; et al. CMS Collaboration

A search for charged Higgs bosons produced in vector boson fusion processes and decaying into vector bosons, using proton--proton collisions at root s = 13 TeV at the LHC, is reported. The data sample corresponds to an integrated luminosity of 137 fb(-1) collected with the CMS detector. Events are selected by requiring two or three electrons or muons, moderate missing transverse momentum, and two jets with a large rapidity separation and a large dijet mass. No excess of events with respect to the standard model background predictions is observed. Model independent upper limits at 95% confidence level are reported on the product of the cross section and branching fraction for vector boson fusion production of charged Higgs bosons as a function of mass, from 200 to 3000 GeV. The results are interpreted in the context of the Georgi-Machacek model.

EUROPEAN PHYSICAL JOURNAL C 81[8], 723, 2021. DOI 10.1140/epjc/s10052-0

[P241-2021] "Search for lepton-flavor violating decays of the Higgs boson in the mu tau and e tau final states in proton-proton collisions at root s=13 TeV"

Sirunyan, A. M; Tumasyan, A.; **Chinellato, J. A.*; Tonelli Manganote, E. J.***; et al. CMS Collaboration

A search is presented for lepton-flavor violating decays of the Higgs boson to mu t and et. The dataset corresponds to an integrated luminosity of 137 fb(-1) collected at the LHC in proton-proton collisions at a center-of-mass energy of 13 TeV. No significant excess has been found, and the results are interpreted in terms of upper limits on lepton-flavor violating branching fractions of the Higgs boson. The observed (expected) upper limits on the branching fractions are, respectively, B(H -> mu t) < 0.15(0.15)% and B(H -> e tau) < 0.22(0.16)% at 95% confidence level..

PHYSICAL REVIEW D 104[3], 032013, 2021. DOI 10.1103/PhysRevD.104.032013

[P242-2021] "Search for signatures of sterile neutrinos with Double Chooz"

Almazan, H.; dos Anjos, J. C.; **Gonzalez, L. F. G.*; Kemp, E.***; et al.

We present a search for signatures of neutrino mixing of electron anti-neutrinos with additional hypothetical sterile neutrino flavors using the Double Chooz experiment. The search is based on data from 5 years of operation of Double Chooz, including 2 years in the two-detector configuration. The analysis is based on a profile likelihood, i.e. comparing the data to the model prediction of disappearance in a data-to-data comparison of the two respective detectors. The analysis is optimized for a model of three active and one sterile neutrino. It is sensitive in the typical mass range 5 x 10(-3) eV(2) less than or similar to Delta m(41)(2) less than or similar to 3 x 10(-1) eV(2) for mixing angles downto sin(2) 2 theta(14) greater than or similar to 0.02. No significant disappearance additionally to the conventional disappearance related to theta(13) is observed and correspondingly exclusion bounds on the sterile mixing parameter theta(14) as a function of Delta m(41)(2) are obtained.

EUROPEAN PHYSICAL JOURNAL C 81[8], 775, 2021. DOI 10.1140/epjc/s10052-021-09459-0

[P243-2021] "Search for top squark production in fully hadronic final states in proton-proton collisions at root s=13 TeV"

Sirunyan, A. M; Tumasyan, A.; **Chinellato, J. A.*; Tonelli Manganote, E. J.***; et al. CMS Collaboration

A search for production of the supersymmetric partners of the top quark, top squarks, is presented. The search is based on proton-proton collision events containing multiple jets, no leptons, and large transverse momentum imbalance. The data were collected with the CMS detector at the CERN LHC at a center-of-mass energy of 13 TeV, and correspond to an integrated luminosity of 137 fb(-1). The targeted signal production scenarios are direct and gluino-mediated top squark production, including scenarios in which the top squark and neutralino masses are nearly degenerate. The search utilizes novel algorithms based on deep neural networks that identify hadronically decaying top quarks and W bosons, which are expected in many of the targeted signal models. No statistically significant excess of events is observed relative to the expectation from the standard model, and limits on the top squark production cross section are obtained in the context of simplified supersymmetric models for various production and decay modes. Exclusion limits as high as 1310 GeVare established at the 95% confidence level on the mass of the top squark for direct top squark production models, and as high as 2260 GeV on the mass of the gluino for gluino-mediated top squark production models. These results represent a significant improvement over the results of previous searches for supersymmetry by CMS in the same final state.

PHYSICAL REVIEW D 104[5], 052001, 2021. DOI: 10.1103/PhysRevD.104.052001

[P244-2021] "Search for top squarks in final states with two top quarks and several light-flavor jets in proton-proton collisions at root s=13 TeV"

Sirunyan, A. M; Tumasyan, A.; **Chinellato, J. A.*; Tonelli Manganote, E. J.***; et al. CMS Collaboration

Many new physics models, including versions of supersymmetry characterized by R-parity violation (RPV), compressed mass spectra, long decay chains, or additional hidden sectors, predict the production of events with top quarks, low missing transverse momentum, and many additional quarks or gluons. The results of a search for new physics in events with two top quarks and additional jets are reported. The search is performed using events with at least seven jets and exactly one electron or muon. No requirement on missing transverse momentum is imposed. The study is based on a sample of proton--proton collisions at root s = 13TeV corresponding to 137 fb(-1) of integrated luminosity collected with the CMS detector at the LHC in 2016-2018. The data are used to determine best fit values and upper limits on the cross section for pair production of top squarks in scenarios of RPV and stealth supersymmetry.

Top squark masses up to 670 (870) GeV are excluded at 95% confidence level for the RPV (stealth) scenario, and the maximum observed local signal significance is 2.8 standard deviations for the RPV scenario with top squark mass of 400 GeV.

PHYSICAL REVIEW D 104[3], 032006, 2021. DOI 10.1103/PhysRevD.104.032006

[P245-2021] "Shannon information criterion for low-high diversity transition in Moran and voter models"

Franco, G. D.*; Marquitti, F. M. D.*; Fernandes, L. D.; Braha, D.; **Aguiar, M. A. M. de***

Mutation and drift play opposite roles in genetics. While mutation creates diversity, drift can cause gene variants to disappear, especially when they are rare. In the absence of natural selection and migration, the balance between the drift and mutation in a well-mixed population defines its diversity. The Moran model captures the effects of these two evolutionary forces and has a counterpart in social dynamics, known as the voter model with external opinion influencers. Two extreme outcomes of the voter model dynamics are consensus and coexistence of opinions, which correspond to low and high diversity in the Moran model. Here we use a Shannon's information-theoretic approach to characterize the smooth transition between the states of consensus and coexistence of opinions in the voter model. Mapping the Moran into the voter model, we extend the results to the mutation-drift balance and characterize the transition between low and high diversity in finite populations. Describing the population as a network of connected individuals, we show that the transition between the two regimes depends on the network topology of the population and on the possible asymmetries in the mutation rates.

PHYSICAL REVIEW E 104[2], 024315, 2021. DOI 10.1103/PhysRevE.104.024315

[P246-2021] "Silicon Microchannel-Driven Raman Scattering Enhancement to Improve Gold Nanorod Functions as a SERS Substrate toward Single-Molecule Detection"

Bar, J.; Barros, A. de; Camargo, D. H. S.; Pereira, M. P.; Merces, L.; **Shimizu, F. M.***; Sigoli, F. A.; Bufon, C. C. B.; Mazali, I. O.

The investigation of enhanced Raman signal effects and the preparation of high-quality, reliable surface-enhanced Raman scattering (SERS) substrates is still a hot topic in the SERS field. Herein, we report an effect based on the shape-induced enhanced Raman scattering (SIERS) to improve the action of gold nanorods (AuNRs) as a SERS substrate. Scattered electric field simulations reveal that bare V-shaped Si substrates exhibit spatially distributed interference patterns from the incident radiation used in the Raman experiment, resulting in constructive interference for an enhanced Raman signal. Experimental data show a 4.29 increase in Raman signal intensity for bare V-shaped Si microchannels when compared with flat Si substrates. The combination of Vshaped microchannels and uniform aggregates of AuNRs is the key feature to achieve detections in ultra-low concentrations, enabling reproducible SERS substrates having high performance and sensitivity. Besides SIERS effects, the geometric design of Vshaped microchannels also enables a "trap" to the molecule confinement and builds up an excellent electromagnetic field distribution by AuNR aggregates. The statistical projection of SERS spectra combined with the SIERS effect displayed a silhouette coefficient of 0.83, indicating attomolar (10-18 mol L-1) detection with the V-shaped Si microchannel.

ACS APPLIED MATERIALS & INTERFACES 13[30], 36482-36491, 024315, 2021. DOI 10.1021/acsami.1c08480

[P247-2021] "Single-Electron Tunneling PbS/InP Heterostructure Nanoplatelets for Synaptic Operations"

Jarschel, P.*; Kim, J. H.; Biadala, L.; Berthe, M.; Lambert, Y.; Osgood, R. M.; Patriarche, G.; Grandidier, B.; Xu, J.

Power consumption, thermal management, and wiring challenge of the binary serial architecture drive the search for alternative paradigms to computing. Of special interest is neuromorphic computing, in which materials and device structures are designed to mimic neuronal functionalities with energy-efficient non-linear responses and both short- and long-term plasticities. In this work, we explore and report on the enabling potential of single-electron tunneling (SET) in PbS nanoplatelets epitaxially grown in the liquid phase on InP, which present these key features. By extrapolating the experimental data in the SET regime, we predict and model synaptic operations. The low-energy (<fJ), high-speed (MHz) operation and scalable fabrication process of the PbS/InP nanoplatelets make such a nanoscale system attractive as neuromorphic computing building blocks.

ACS APPLIED MATERIALS & INTERFACES 13[32], 38450-38457, 032006, 2021. DOI 10.1021/acsami.1c06096

[P248-2021] "Small difference between the nonlinear refractions of normal and deuterated solvents measurable by nonlinear ellipse rotation"

Fernandes, J. C.; Barbano, E. C.; **Siqueira, J. P.*;** Misoguti, L.

In this work, we have measured the nonlinear refractions of six different normal and deuterated solvents: water, DMSO, methanol, acetone, toluene, and chloroform using a nonlinear ellipse rotation (NER) signal with femtosecond laser pulses. High-precision, self-referenced NER measurements could detect small differences between the refractive nonlinearities of normal and deuterated solvents. We observed that the replacement of hydrogen with deuterium atoms slightly reduces the magnitude of the nonlinearity. Basically, the reduction is related to the amount of hydrogen and the replacement by deuterium atoms in the molecules; in this way, toluene (chloroform) presents the major (minor) difference. By measuring the nonlinear refraction as a function of the pulse width, we also could observe that the refractive nonlinearity increases as the pulse gets longer. Using a simple empirical model, we could discriminate the ultrafast electronic and delayed orientational refractive nonlinearities of these six pairs of solvents.

JOURNAL OF THE OPTICAL SOCIETY OF AMERICA B-OPTICAL PHYSICS 38[9], 2663-2668, 138919, 2021. DOI 10.1364/JOSAB.423211

[P249-2021] "Structure, Properties and Applications of Two-Dimensional Hexagonal Boron Nitride"

Roy, S.; Zhang, X.; **Oliveira, E. F.*;** et al.

Hexagonal boron nitride (h-BN) has emerged as a strong candidate for two-dimensional (2D) material owing to its exciting optoelectrical properties combined with mechanical robustness, thermal stability, and chemical inertness. Super-thin h-BN layers have gained significant attention from the scientific community for many applications, including nanoelectronics, photonics, biomedical, anti-corrosion, and catalysis, among others. This review provides a systematic elaboration of the structural, electrical, mechanical, optical, and thermal properties of h-BN followed by a comprehensive account of state--of-the-art synthesis strategies for 2D h-BN, including chemical exfoliation, chemical, and physical vapor deposition, and other methods that have been successfully developed in recent years.

It further elaborates a wide variety of processing routes developed for doping, substitution, functionalization, and combination with other materials to form heterostructures. Based on the extraordinary properties and thermal--mechanical-chemical stability of 2D h-BN, various potential applications of these structures are described.

ADVANCED MATERIALS, 2101589. Acesso antecipado SEP 2021. DOI: 10.1002/adma.202101589

[P250-2021] "Superconductivity in highly doped diamond: Role of group III and V impurities"

Costa, F. J. R.*; Almeida, J. S. de

This study comprises an investigation of the superconductivity in highly doped diamond, comprising elements from groups III and V acting as acceptor and donor impurities, respectively, within the virtual crystal approximation. Calculations of the electron-phonon coupling were carried out for each case, enlightening the different aspects arising from different doping elements and their consequent impact on the superconducting critical temperature. These calculations indicated that among the hole-doped cases the electron-phonon coupling is strongly related to the optical phonons of the lattice. Regarding the electron-doped systems, it was observed that the coupling had contributions from both optical and acoustic vibrations, leading to high estimates for the critical temperature. Through the comparison between these opposing scenarios, several distinctions between the electron- and hole-doped cases became evident, implying that the mechanisms of superconductivity in doped diamond relate directly to the nature of the impurity added to the system. These results provide further evidence that the electronic and dynamic changes arising from the electron doping of a diamond may lead to superconductivity in high temperatures. Published under an exclusive license by AIP Publishing.

JOURNAL OF APPLIED PHYSICS 130[4], 043903, 2021. DOI 10.1063/5.0055633

[P251-2021] "Synthesis, characterization and in vitro cytotoxicity study of Co and Ni ferrite nanoparticles prepared by sol-gel method"

Pancotti, A.; Santos, D. P.; Morais, D. O.; Souza, M. V. D.; Lima, D. R.; Vulcani, V. A. S.; Martins, A.; **Landers, R.***; Braoios, A.

In this study, we report the synthesis and characterization of NiFe2O4 and CoFe2O4 nanoparticles (NPs) which are widely used in the biomedical area. There is still limited knowledge how the properties of these materials are influenced by different chemical routes. In this work, we investigated the effect of heat treatment over cytotoxicity of cobalt and niquel ferrites NPs synthesized by sol-gel method. Then the samples were studied using transmission electron microscopy (TEM), X--ray diffraction (XRD), X-ray photoelectron spectroscopy (XPS), vibrating sample magnetometer (VSM), Fourier Transform Infrared Spectroscopy Analysis (FTIR), and X-ray fluorescence (XRF). The average crystallite sizes of the particles were found to be in the range of 20-35 nm. The hemocompatibility (erythrocytes and leukocytes) was checked. Cytotoxicity results were similar to those of the control test sample, therefore suggesting hemocompatibility of the tested materials.

SN APPLIED SCIENCES 3[7], 716, 2021. DOI 10.1007/s42452-021-04709-y

[P252-2021] "Systematic comparison of various oxidation treatments on diamond surface"

Li, C. X.; Zhang, X.; **Oliveira, E. F.***; Puthirath, A. B.; Neupane, M. R.; Weil, J. D.; Birdwell, A. G.; Ivanov, T. G.; Kong, S.;; Gray, T.; Kannan, H.; Biswas, A.; Vajtai, R.; **Galvao, D. S.***; Ajayan, P. M.

It is known that surface terminations contribute significantly to diamond properties. As one of the most commonly studied types, oxygen-terminated diamond surface possesses a positive electron affinity (PEA) and hydrophilicity, making it suitable for electronic device fabrication and bioapplications. Various oxidation methods have been reported on diamond, but a systematic comparison is still lacking. Herein, we present a comparative study on the oxidation of microcrystalline diamond powder (DP) and polycrystalline diamond film (PCD) by wet chemical treatments, including various acid mixtures, as well as by dry processes, including O-2 plasma and UV ozone. X-ray photoelectron spectroscopy (XPS) and Fourier-transform infrared spectroscopy (FTIR) results reveal that H2SO4/HNO3 5:1 at 360 degrees C demonstrates the best oxidation performance on DP and PCD compared to other wet chemical methods, while the PCD treated by O-2 plasma exhibits the highest oxygen content among all the treated samples. Besides, the concentration of carbon-oxygen groups on diamond surfaces is found largely determined by oxidation methods. These experimental results can be attributed to the corresponding oxidation mechanism of different treatments and agree well with theoretical simulations. Finally, we investigated the sp(2) bonded carbon concentration and surface roughness of oxidized PCD, suggesting the optimized diamond surface cleaning conditions.

CARBON 182, 725-734, 2021. DOI 10.1016/j.carbon.2021.06.050

[P253-2021] "Tannin-based carbon xerogel as a promising co-catalyst for photodegradation processes based on solar light: a case study using the tin (IV) oxide/carbon xerogel composite"

Moraes, N. P. de; Goes, C. M.; Rocha, R. D.; Gouvea, M. E. V.; **Siervo, A. de***; Silva, M. L. C. P. da; Rodrigues, L. A.

This work aimed to evidence the potential use of tannin-based carbon xerogel as a co-catalyst in photocatalytic processes based on solar light. Specifically, the tin (IV) oxide/carbon xerogel photocatalyst (SnO2/XC) was developed with the objective of improving the photoactivity of tin (IV) oxide (SnO2) under simulated solar light. The photocatalytic efficiency was determined by the degradation of the 4-chlorophenol molecule. The synthesis proposed in this work is based on a simple one-pot precipitation reaction, using black wattle tannin and tin chloride as precursors. The materials synthesized were characterized by X-ray diffractometry, diffuse reflectance spectroscopy, infrared spectroscopy, X-ray photoelectron spectroscopy, energy dispersive spectroscopy, scanning electron microscopy, adsorption isotherms, and chronoamperometry. Results showed the presence of tetragonal SnO2 in the samples synthesized. Carbon xerogel addition led to an increased specific surface area (55% higher) and lower bandgap energy (from 3.64 eV to 3.58 eV). The photocatalytic evaluation shows that the SnO2/XC composite has superior photocatalytic efficiency (44% removal vs 20% for the SnO2), obtaining a reaction rate constant (k(app) = 0.00172 min(-1)) which is nearly double the one obtained by the pure SnO2 (k(app) = 0.00096 min(-1)). The chronoamperometric results indicated that the proposed modification enhanced the photocurrent generation and charge separation in the SnO2/XC, facilitating the formation of active radicals during the process and further degrading the reaction intermediates formed during the photodegradation process.

CHEMICAL ENGINEERING COMMUNICATIONS, Acesso antecipado SEP 2021. DOI 10.1080/00986445.2021.1978076

[P254-2021] "The FRAM robotic telescope for atmospheric monitoring at the Pierre Auger Observatory"

Aab, A.; Abreu, P.; **Chinellato, J. A.*; Franco D. de O.*; Dobrigkeit, C.*; Fauth, A. C.*; Payeras, A. M.*; Muller, M. A.*;** et al. Pierre Auger Collaboration

FRAM (F/Photometric Robotic Atmospheric Monitor) is a robotic telescope operated at the Pierre Auger Observatory in Argentina for the purposes of atmospheric monitoring using stellar photometry. As a passive system which does not produce any light that could interfere with the observations of the fluorescence telescopes of the observatory, it complements the active monitoring systems that use lasers. We discuss the applications of stellar photometry for atmospheric monitoring at optical observatories in general and the particular modes of operation employed by the Auger FRAM. We describe in detail the technical aspects of FRAM, the hardware and software requirements for a successful operation of a robotic telescope for such a purpose and their implementation within the FRAM system.

SN APPLIED SCIENCES 3[7], 716, 2021. DOI 10.1007/s42452-021-04709-y

[P255-2021] "Unruh-DeWitt detector in AdS(2)"

Pitelli, J. P. M.; **Felipe, B. S.*;** Mosna, R. A.

We find the response function and the transition rate for an Unruh-DeWitt detector interacting with a conformal scalar field in global two-dimensional anti-de Sitter (AdS) spacetime with different boundary conditions at its conformal infinities. We calculate the particle energy spectrum as seen by subcritical accelerated detectors and discuss how it depends on the choice of the boundary condition. We show that, despite this nontrivial dependence on the boundary conditions, the limit when the AdS length scale tends to zero is well defined and leads to the well-known results of 1 + 1 Minkowski space. One can thus interpret the AdS energy scale as a natural regulator for the well-known infrared ambiguity of massless scalar fields in 1 + 1 Minkowski spacetime.

PHYSICAL REVIEW D 104[4], 045008, 2021. DOI 10.1103/PhysRevD.104.045008

[P256-2021] "Using Wikiversity in teaching scientific journalism: openness, collaboration and connectivism"

Dieb, D. A. A.; Peschanski, J. A.; **Paixao, F. J. da***

This article aims at critically presenting a case study about the creation of an online, open and collaborative course of introduction to scientific journalism. It begins showing the context in which the project was conceived and then briefly talks about the triad "communication, education and technology", emphasizing technology's role in distance education, which can be seen from the historical perspective of "generations of technological innovation". In the current context, with the Internet's advent and practices related to the 2.0 Web, this case deepens the description of a course, hosted at Wikiversity, and on its creation processes.

TEXTO LIVRE-LINGUAGEM E TECNOLOGIA 14[1], e24935, 2021. DOI 10.35699/1983-3652.2021.24935

Meeting Abstract

[Me001-2021] "Implementation of Detailed Monte Carlo Simulation for Semiconductor Detectors Using the PENELOPE Code"

Mendes, H.*; Tomal, A.*

MEDICAL PHYSICS 48[6], Resumo do encontro MO-IePD-TR, Número do artigo 165378, Publicado JUN 2021.

Correções

[Co007-2021] "Invisible neutrino decay: first vs second oscillation maximum (May, 10.1007/JHEP05(2021)091, 2021)"

Chakraborty, K.; Dutta, D.; Goswami, S.; **Pramanik, D.***

JOURNAL OF HIGH ENERGY PHYSICS [8], 136, 2021. DOI 10.1007/jhep08(2021)136

[Co008-2021] "Unconventional enhancement of ferromagnetic interactions in Cd-doped GdFe2Zn20 single crystals studied by ESR and Fe-57 Mossbauer spectroscopies (vol 102, 144420, 2020)"

Cabrera-Baez, M.; Munevar, J.; Couto-Mota, R. M.; Camejo, Y. M.; Contreras, C.; Baggio-Saitovitch, E.; Avila, M. A.; **Rettori, C.***

Physical Review B 103[17], 179903, 2021. DOI 10.1103/PhysRevB.103.179903

***Autores da comunidade IFGW**
Fonte: Web of Science on-line (WOS)

Defesas de Dissertações do IFGW

[D016-2021] "Construção e validação de um sistema óptico para medidas cerebrais em ambientes naturais"
Aluno: Giovanni Hering Scavariello
Orientador: Prof. Dr. Rickson Coelho Mesquita
Data: 23/09/2021

[D017-2021] "Estudo Exploratório da Função de Green Não Perturbativa do Vértice de Quatro Pontos no Formalismo de Background Field"
Aluno: Bianca Maria S. de Oliveira
Orientador: Profa. Dra. Arlene Cristina Aguilar
Data: 29/09/2021

[D018-2021] "Estudo dos Relógios Quânticos por meio de Analogias com Relógios em um Campo Gravitacional"
Aluno: Wanderson Costa Oliveira
Orientador: Prof. Dr. Pierre-Louis de Assis
Data: 30/09/2021

[D019-2021] "Diferenciação de orbital via acoplamento hiperfino em 63Cu"
Aluno: Davi Antonio Zau de Alvarenga
Orientador: Prof. Dr. Ricardo Urbano
Data: 11/10/2021

Defesas de Teses do IFGW

[T012-2021] "ARAPUCA, dispositivo de coleta de luz para o experimento DUNE"
Aluno: Henrique Vieira de Souza
Orientador: Prof. Dr. Ettore Segreto
Data: 23/09/2021

[T013-2021] "Os muitos vácuos de AdS2 via detector de Unruh-DeWitt"
Aluno: Bruno Santos Felipe
Orientador: Prof. Dr. João Paulo Pitelli Manoel
Data: 24/09/2021

Fonte: Portal IFGW/Pós-graduação - Agenda de Colóquios, Defesas e Seminários.
Disponível em: http://portal.ifi.unicamp.br/pos-graduacao

Defesas de Teses e Dissertações do PECIM

Observação: Não ocorreram neste período defesas de teses e dissertações, com orientadores ou banca do IFGW, do Programa de Pós-Graduação Multiunidades em Ensino de Ciências e Matemática – Mestrado e Doutorado (PECIM) da Unicamp.

Fonte: Página do PECIM
Disponível em: https://www.pecim.unicamp.br/bancas

Abstracta

Instituto de Física "Gleb Wataghin" - IFGW
Diretora: Profa. Dra. Mônica Alonso Cotta
Diretor Associado: Prof. Dr. Marcos Cesar de Oliveira
Universidade Estadual de Campinas - UNICAMP
Cidade Universitária Zeferino Vaz
13083-859 - Campinas - SP - Brasil
e-mail: secdir@ifi.unicamp.br
Fone: +55 19 3521-5300

Publicação

Biblioteca do Instituto de Física Gleb Wataghin
http://portal.ifi.unicamp.br/biblioteca

Diretora Técnica: Sandra Maria Carlos Cartaxo
Coordenadora da Comissão de Biblioteca: Profa. Dra. Arlene Cristina Aguilar

Elaboração:
Maria Graciele Trevisan (Bibliotecária)
Ayres Neri da Cunha Junior (Técnico Administrativo)
contato: infobif@ifi.unicamp.br